Influence of Solubility on Twin-Screw Multiphase Pumps Conveying Oil and Gas

Dipl.-Wirtsch.-Ing. T. Groth, Dipl.-Wirtsch.-Ing. F. Hatesuer, Prof. Dr.-Ing. A. Luke
Institute of Thermodynamics, Leibniz University of Hannover, Germany

Prof. Dr.-Ing. Dr.h.c. D. Mewes
Institute of Multiphase Processes, Leibniz University of Hannover, Germany

Dipl.-Ing. G. Rohlfing, Dipl.-Ing. M. Reichwage
Johann Heinrich Bornemann GmbH, Obernkirchen, Germany

ABSTRACT

Twin-screw pumps are employed to convey multi-phase flows of crude oil, natural gas and accompanying fluids or even solid particles. The solubility of gas in oil affects the gas fraction and the pressure along the conveying process and thus the operation conditions. In this paper, the delivering behaviour and the flow characteristics of a twin-screw multiphase pump (MPP) conveying two-phase mixtures of oil, air and carbon dioxide, are investigated experimentally. Further, the solubilities of air, carbon dioxide and methane in oil are calculated and a dissolution model of the MPP is derived. High solubility is found to decrease the delivering performance and to reduce the gas fraction in the outlet pipe.

NOMENCLATURE

General symbols

a	parameter, J m^3 kg^{-1} mol^{-1} K^{-1}
b	parameter, m^3 kg^{-1}
C	function of inlet and outlet conditions, -
g^E	Gibbs excess enthalpy, J
H	Henry coefficient, bar
M	molar mass, kg $kmol^{-1}$
N	number of screws, -
n	rotational frequency, min^{-1}
p	pressure, bar
R_i	individual gas constant, J kg^{-1} K^{-1}
T	temperature, K
t	time, s
$\dot{V}$	volume flow, m^3 h^{-1}
v	specific volume, m^3 kg^{-1}
x	molar fraction, -
α	gas volume fraction, -
ά	gas volume flow fraction, -
Υ	activity coefficient, -
η	efficiency, -
λ	solubility coefficient, l_n kg^{-1}
ρ	density, kg m^{-3}

Subscripts

1	status 1
2	status 2
ch	chamber
comb	combinatorial
deg	degassing
gas	gas
gap	gap
i	component i
in	inlet
loss	loss
MPP	multiphase pump
m	measured
n	norm conditions (0 °C, 1 bar)
oil	oil
out	outlet
rec	recirculation

Dipl.-Wirtsch.-Ing. T. Groth, Dipl.-Wirtsch.-Ing. F. Hatesuer, Prof. Dr.-Ing. A. Luke, Prof. Dr.-Ing. Dr.h.c. D. Mewes, Dipl.-Ing. G. Rohlfing, Dipl.-Ing. M. Reichwage

res	residual
s	shaft
T	isothermal
th	theoretical
vol	volumetric

1 INTRODUCTION

Twin-Screw multiphase pumps (MPPs) are employed in the oil and gas production industry in order to increase the efficiency and yield of fields in offshore and onshore regions (1). Two-phase gas-liquid flows of highly viscous fluids are conveyed even at high gas rates without separation (2). Cost-intensive processing units close to the wellheads and gas-flaring are avoided. Remote and difficult to access or marginal fields are made available (3). Conventionally depleted fields are further exploited (4).

As main influence parameters on the delivery behaviour of MPPs the boosted pressure difference, the rotational frequency and the gas volume flow fraction are found (5). The experimental results for water/air indicate increasing volumetric efficiency if the gas fraction is increased up to 95 percent or the rotational frequency is risen, as the gap sealing is enhanced and the loss is minimized (6). At very high gas fractions, the volumetric efficiency drops due to the passover of gas in the gaps (7), as sealing fails due to the lack of liquid. For oil/air less experimental results than for water/air are published. The available data of oil/air indicates comparable results to water/air regarding the influence of the pressure difference, the gas fraction and the rotational frequency. The volume flow tends to decrease by rising the gas fraction above 75 percent. Increasing the viscosity of oil by reducing the temperature is found to increase the volume flow, but to decrease the absorbed power and the isothermal efficiency (8).

Modelling the delivering behaviour is presented by Mewes et al. (9). They derive a model based on energy and mass balances in order to estimate the pressure profile determining the loss and mechanical load for various operating points. The calculated pressure profiles match the experimental data and are used to predict the delivered volume flow.

Nakashima et al. (10) simulate a MPP by a separator, compressor, pump and mixer. They calculate the influence of the gas fraction and the rotational frequency on the pressure profile, the loss and the power. An increasingly progressive pressure profile is found for rising gas fractions and rising rotational frequencies.

In literature, the influence of solubility on multiphase boosting is hardly considered. Hellmann (11) presents equations of the gas volume in two-phase gas-liquid flows due to pressure increase in pumps or pressure decrease in turbines. He calculates the solubility by means of the law of Henry.

Since in the on hand work the liquid oil phase contains dissolved gas, the gas rate along the conveying process is affected by the variable solubility of gas in oil. With increasing pressure and decreasing temperature the solubility rises and dissolving occurs. Inside of twin-screw multiphase pumps, the pressure in the conveyed volume flow is increased, while the pressure is decreased in the counterstreaming gap flows. As a consequence, degassing occurs and the phase fractions as well as the flow patterns around the screws and in the inlet and outlet pipe are affected.

In Figure 1 the intermeshing twin-screws and the volume flows around them are drawn. Due to the pressure difference between the inlet and outlet, gas is dissolved inside the chambers moving the volume flow $\dot{V}$ from the left to the right. In the gap volume flows $\dot{V}_{gap}$ streaming contrary to $\dot{V}$, degassing occurs and increases the gas volume. The gap flows are decelerated by the flow inside the chambers, which is influenced by the rotational frequency of the screws, the fluid properties and the gas fraction. In dependence of these influence parameters, the gaps are more or less sealed with liquid and the total pressure is distributed along the screw. The resulting pressure profile and the phase fractions, which appear in the gaps, determine the loss volume flow $\dot{V}_{loss}$.

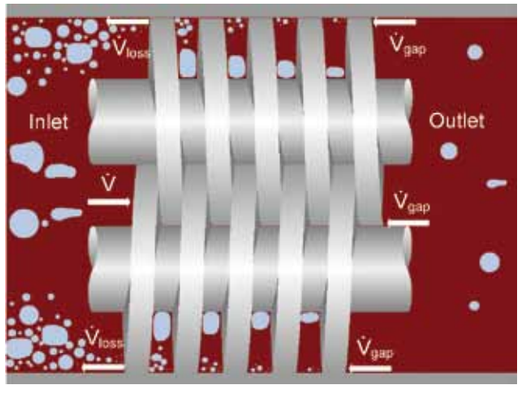

Figure 1: Volume flows around the twin screws

Degassing of air-saturated oil inside a screw model is observable, as shown in Figure 2. The transparent casing, containing the screw model and bordering together with the screw flanks the conveying chamber, is completely filled with air-saturated oil only. The initial gas fraction is zero. At 10 s after starting the screw rotation and setting the gap flow, gas bubbles appear in the conveying chamber and the inlet chamber. After 20 s, dispersed gas bubbles govern the phase distribution and at 30 s, phases tend to separate and gas begins to enter the gap.

The influence of degassing and dissolution on the delivery behaviour and on the flow characteristics is investigated in the following.

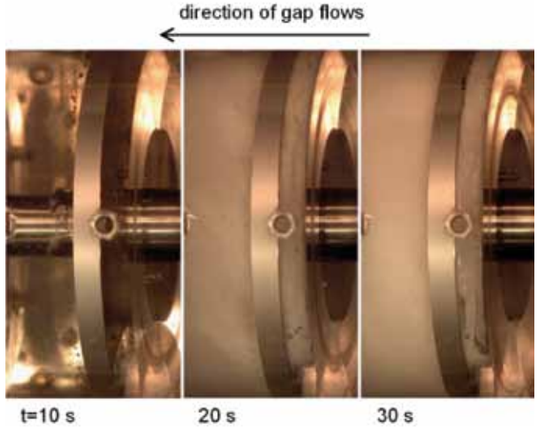

Figure 2: Degassing in a conveying chamber model

2 THEORETICAL REGARD

The delivering behaviour is described by the equations of the conveyed volume flow, the volumetric and isothermal efficiency regarding the solubility. In order to obtain these quantities, the loss volume flow and the absorbed power have to be calculated in dependence of the boundary conditions. Considering sorption phenomena, the solubility of different gases in oil is calculated as a function of pressure and temperature to determine the influence on the delivering behaviour.

2.1 Calculating the solubility

The solubility can be estimated by using the law of Henry (12), which approaches the soluble gas fraction x_i as linearly dependent on the partial pressure p_i, which equals approximately the total pressure of the gas phase:

$$p_i = H \cdot x_i \qquad (1)$$

H represents the coefficient of Henry which is obtained from literature (13). Since the regarded gases methane and carbon dioxide are highly soluble, the more accurate Predictive-Soave-Redlich-Kwong (PSRK) model is applied (14). Based on the thermal equation of state by Soave-Redlich-Kwong

Dipl.-Wirtsch.-Ing. T. Groth, Dipl.-Wirtsch.-Ing. F. Hatesuer, Prof. Dr.-Ing. A. Luke, Prof. Dr.-Ing. Dr.h.c. D. Mewes, Dipl.-Ing. G. Rohlfing, Dipl.-Ing. M. Reichwage

$$p = \frac{R_i T}{v-b} - \frac{a(T)}{v(v+b)} \qquad (2)$$

which gives the relation between the pressure p, the temperature T, the specific volume v and the individual gas constant Ri in dependence of the mixing parameters a and b. a and b are calculated by means of the complex mixing rule

$$\frac{a(T)}{bRT} = \sum_i x_i \frac{a_i(T)}{b_i RT} + \frac{\frac{g^E}{RT} + \sum_i x_i \ln\frac{b}{b_i}}{-0.64663} \qquad (3)$$

where a_i and b_i represent the mixing parameters of each component i (15). a_i and b_i are calculated from the properties of the pure components. The Gibbs excess enthalpy g^E is derived from the individual activity coefficients γ_i by:

$$g^E = RT\sum_i x_i \ln\gamma_i \qquad (4)$$

The individual activity coefficients are calculated according to UNIQUAC of the combinatorial and residual fraction (16):

$$\ln\gamma_i = \ln\gamma_i^{comb} + \ln\gamma_i^{res} \qquad (5)$$

In Figure 3 the calculated solubilities of air (regarded as nitrogen), methane and carbon dioxide in paraffinic white oil are presented for constant temperature. The continuous-lined curves represent the solubilty as functions of the pressure resulting from PSRK. The dashed lines result from the law of Henry by conversion with the molar masses of gas and liquid and the specific norm volume (17):

$$\lambda_{gas} = p \cdot H^{-1}(T) \cdot M_{oil}^{-1} \cdot v_n \cdot M_{gas} \qquad (6)$$

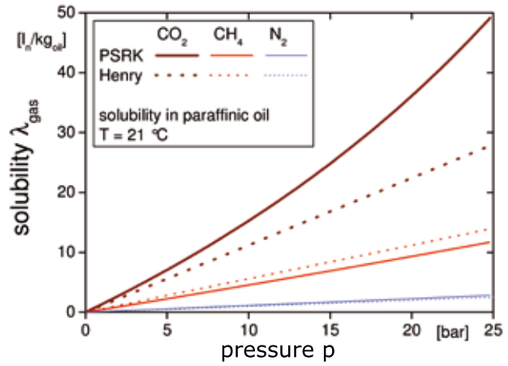

Figure 3: Calculated solubility of different gases

The highest solubility in paraffinic oil is found for carbon dioxide, the lowest for nitrogen. The solubility of methane is between both. Comparing the PSRK model and the law of Henry, large deviations exist for CO_2 at nearly all pressures. For CH_4 there are still significant deviations at high pressures, while the deviation for N_2 is negligible. The solubility functions λ_{gas} (p) are implemented into the equations of the delivering behaviour.

2.2 Equations of the delivering behaviour

The conveyed volume flow $\dot{V}$ of two-phase gas-liquid mixtures at inlet conditions

$$\dot{V} = \dot{V}_{th} - \dot{V}_{loss} - \dot{V}_{rec} \qquad (7)$$

is defined as the theoretically displaced volume flow $\dot{V}_{th}$ minus the loss $\dot{V}_{loss}$ and recirculation volume flow $\dot{V}_{rec}$. $\dot{V}_{rec}$ is an internal parameter to enhance the gap sealing (18). $\dot{V}_{th}$ is determined by the chamber volume V_{ch}, the number of screws N and the rotational frequency n:

$$\dot{V}_{th} = N \cdot n \cdot V_{ch} \qquad (8)$$

Regarding the phase volume flows, $\dot{V}$ is expressed by:

$$\dot{V} = \dot{V}_{gas} + \dot{V}_{oil} \qquad (9)$$

The inlet oil volume flow $\dot{V}_{oil}$ equals the measured one, assuming oil as an incompressible liquid. The inlet gas volume flow $\dot{V}_{gas}$ is composed of the measured gas volume flow $\dot{V}_{gas,m}$, on the one hand, and the considered degassing norm volume flow $\dot{V}_{deg,n}$ due to the pressure drop before the inlet, on the other hand. Both, measured and degassing volume flows, are converted to inlet conditions (p_{in}, T_{in}) by the ideal gas law

$$\dot{V}_{gas} = \frac{p_m}{p_{in}}\frac{T_{in}}{T_m} \cdot \dot{V}_{gas,m} + \frac{p_n}{p_{in}}\frac{T_{in}}{T_n} \cdot \dot{V}_{deg,n} \qquad (10)$$

where (p_m, T_m) represent the conditions at the sensor position and (p_n, T_n) represent norm conditions. Implementing the solubility functions brings

$$\dot{V}_{deg,n} = \rho_{oil}(T_{in}) \cdot \dot{V}_{oil} \cdot (\lambda_{gas}(p_m) - \lambda_{gas}(p_{in})) \qquad (11)$$

where the oil density at inlet conditions $\rho_{oil}(T_{in})$ is needed for the accurate calculation of the degassing volume. Hence, the conveyed volume flow considering degassing before the inlet is obtained. The volumetric efficiency η_{vol}

$$\eta_{vol} = \frac{\dot{V}}{\dot{V}_{th}} \qquad (12)$$

is defined as the ratio of conveyed volume flow and the theoretical one. Taking into account the higher heat capacity and density of oil and the intensive contact of gas and liquid phase, isothermal boosting is assumed and the isothermal efficiency η_T is used to express efficiency:

$$\eta_T = \left(\dot{V}_{oil} \cdot \Delta p_{MPP} + \dot{V}_{gas} \cdot p_{in} \cdot \ln\frac{p_{out}}{p_{in}}\right) P_s^{-1} \qquad (13)$$

η_T is defined as the sum of the isothermal compression powers of each phase divided by the absorbed shaft power P_s. The influence of dissolution and degassing inside the MPP on the flow characteristics at the inlet and outlet, given in Figure 4, is modelled.

Figure 4: Modelling the flow characteristics

The assumptions of modelling are, as already discussed above, isothermal boosting

$$T_{out} = T_{in} \qquad (14),$$

incompressible oil phase

$$\dot{V}_{oil,out} = \dot{V}_{oil,in} = \dot{V}_{oil} \qquad (15)$$

and ideal gas phase

$$p_1 \dot{V}_{gas,1} = p_2 \dot{V}_{gas,2} \qquad (16).$$

According to Eq. 9, 10 and 11 and the definition of the gas volume flow fraction $\dot{\alpha}$

$$\dot{\alpha} = \frac{\dot{V}_{gas}}{\dot{V}_{oil} + \dot{V}_{gas}} \qquad (17),$$

the gas volume flow at the outlet

$$\dot{V}_{gas,out} = \dot{V}_{in} \cdot C \qquad (18)$$

is determined as a function of the inlet volume flow and the inlet and outlet conditions C, defined by:

$$C \equiv \dot{\alpha}_{in}\frac{p_{in}}{p_{out}} - \frac{(1-\dot{\alpha}_{in})}{v_{oil}(T_{in})}\frac{p_n T_{in}}{p_{out} T_n}(\lambda_{gas}(p_{out}) - \lambda_{gas}(p_{in})) \qquad (19)$$

The outlet gas volume flow fraction is derived:

$$\dot{\alpha}_{out} = \frac{C(p_{in}, p_{out}, T_{in}, \dot{\alpha}_{in}, \lambda_{gas})}{1 - \dot{\alpha}_{in} + C} \qquad (20)$$

$\dot{\alpha}_{in}$ in Eq. 20 has to meet the following relation, else more gas than present would be dissolved and $\dot{\alpha}_{out}$ would become negative:

$$\dot{\alpha}_{in} \geq \frac{\rho_{oil}\frac{p_n T_{in}}{p_{in} T_n}(\lambda_{gas}(p_{out}) - \lambda_{gas}(p_{in}))}{1 + \rho_{oil}\frac{p_n T_{in}}{p_{in} T_n}(\lambda_{gas}(p_{out}) - \lambda_{gas}(p_{in}))} \qquad (21)$$

The effect of degassing inside the MPP on the inlet gas fraction due to variations of the phase fractions in the loss flow is calculated by Eq. 18. For this purpose, the inlet gap volume flow has to be set instead of $\dot{V}_{in}$ and assumed to be only liquid, gas-saturated oil ($\dot{\alpha}_{in}$=0).

Dipl.-Wirtsch.-Ing. T. Groth, Dipl.-Wirtsch.-Ing. F. Hatesuer, Prof. Dr.-Ing. A. Luke, Prof. Dr.-Ing. Dr.h.c. D. Mewes, Dipl.-Ing. G. Rohlfing, Dipl.-Ing. M. Reichwage

3 EXPERIMENTAL SETUP

The test facility and the measurement of the delivering behaviour as well as the flow characteristics are presented.

3.1 The test facility

The test facility is pictured schematically in Figure 5.

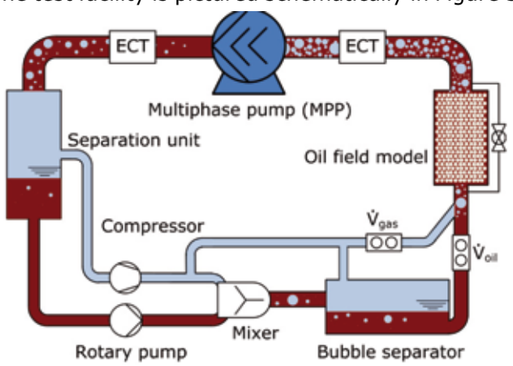

Figure 5: Schematic of the test facility

In essence, it consists of a saturation part, represented by the mixer and bubble separator, an oil field model (which is not regarded in this paper), a MPP, a separation unit and the single-phase conveying elements compressor and rotary pump. The two-phase flow is separated after boosting by the MPP in order to realize a continuous closed-loop mode of operation. The separated flows of oil and gas are conveyed by the rotary pump and the compressor, respectively, and afterwards mixed to assure saturation at variable pressure and temperature. After mixing, the excess gas is separated from the oil. Subsequently, saturated oil and gas are led as two-phase flow with variable phase fractions to the MPP. The gas volume flow fraction and the total volume flow are derived from flow meters measuring $\dot{V}_{gas}$ and $\dot{V}_{oil}$. The gas volume fractions and flow patterns at the inlet and outlet side of the MPP are measured by an electrical capacitance tomography (ECT) system, which is described more detailed later. The corresponding flow chart of the test facility is shown in Figure 6.

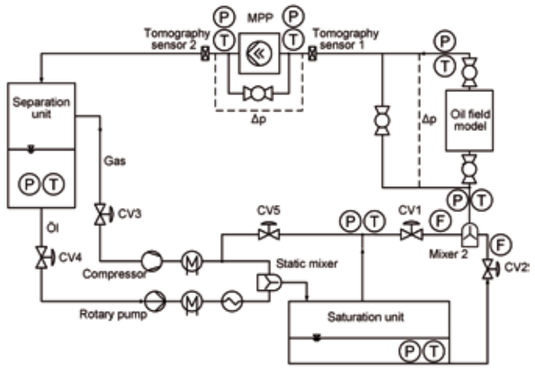

Figure 6: Simplified flow chart of the test facility

The volume flows of oil and gas, on the one hand, are set by the control valves CV1 and CV2. On the other hand, the inlet pressure of the MPP is controlled by CV1 and CV2. The counter pressure of the MPP is set by CV3 and CV4 at the outlet of the separation vessel. After leaving the separation unit both, the gas and oil streams, are boosted and cooled or heated in order to determine the solubility of gas in oil and other thermophysical properties like the viscosity before being mixed. The rotational frequency of all conveying elements is determined by frequency converters. The pump under investigation is a MPC 112/133 twin-screw pump, produced by Bornemann Pumps.

3.2 Measurement

The rotational frequencies, power of the MPP, measured temperatures, pressures, flow rates and derived quantities are processed by means of the software Labview (19). The two-phase flow characteristics are measured online and the raw data is saved for further analysis.

ECT measurement is used for non-conducting fluids. The measurement principle is based on the different electrical permittivities of oil and gas, as given in Figure 7 on the left. The average permittivity between two electrodes is measured by injecting a current and and metering the load and voltage to determine the capacity. Repeating this procedure for all linearly independent combinations of the 12 electrodes delivers the cross-sectional distribution of capacities, from which the phase distribution is derived by means of a linear back projection algorithm (20). The phase distribution is visualised as cross-sectional tomogram (Figure 7 on the right), where gas is represented by blue pixels, oil by red pixels and mixed phase areas (foam) by yellow-green pixels. Further, horizontal and vertical longitudinal cuts are visualized from the same raw data. The applied system provides a spacial resolution of 812 pixels at high temporal resolution. Due to the shielding steel tube, the sensors are pressure resistant up to 16 bar.

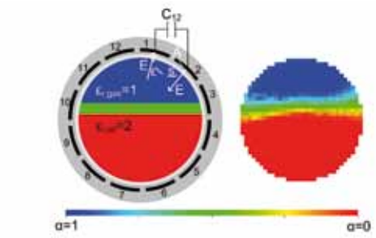

Figure 7: Electrical capacitance tomography

Based on the flow characteristics, the influence of degassing and dissolving inside the MPP is analysed.

4 RESULTS

Primarily, the experimental results of the delivery behaviour are presented to regard the influence of solubility. Secondly, the visualized flow characteristics are discussed regarding the internal phenomena inside the MPP. Finally, the experimental results of the gas fractions are compared to the theoretical ones.

4.1 Delivering behaviour

The measured two-phase inlet volume flow (Eq. 9-11) of oil/air and oil/CO_2 as a function of the pressure difference is shown in Figure 8 for two rotational frequencies. The gas volume flow fraction is varied and the inlet conditions are constant. No volume flow is recirculated.

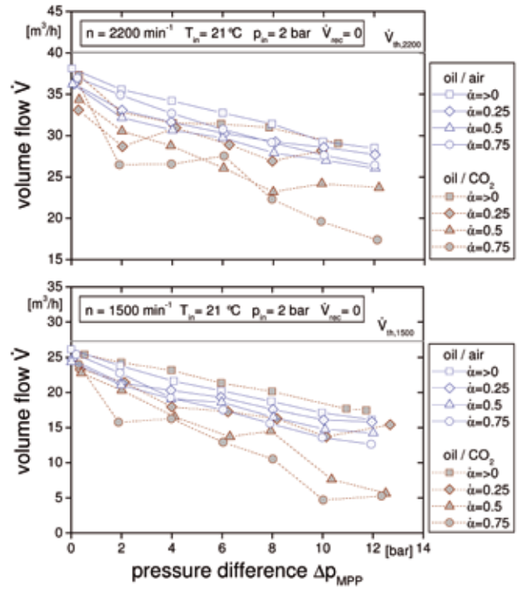

Figure 8: Measured two-phase volume flow of oil/air and oil/CO_2 as a function of the pressure difference at n=2200 and 1500 min^{-1}

The volume flow $\dot{V}$ is decreased by increasing the pressure difference Δp_{MPP} or decreasing the rotational frequency n.

By increasing the gas volume flow fraction $\dot{\alpha}$, $\dot{V}$ is decreased. In contrast to the results of other authors (5, 8), the volume flow is not increased by increasing $\dot{\alpha}$, which is due to the saturation in the on hand investigations. Comparing air to CO_2, the decrease of $\dot{V}$ is stronger for all influence parameters pressure difference, rotational frequency and gas volume flow fraction. In particular at high pressure differences and gas fractions, the oil/CO_2 volume flow slumps. Further, it is very volatile which will be examined more detailed below. This gives reason for assuming a negative influence of high solubility on the conveying process. Referring to Scharf (21), the pressure profile is obviously affected by degassing of the gap flows and the loss volume flow is increased. The absorbed shaft power is hardly affected by the solubility and thus not presented here. The measured isothermal efficiencies (Eq. 13) for oil/air and oil/

Dipl.-Wirtsch.-Ing. T. Groth, Dipl.-Wirtsch.-Ing. F. Hatesuer, Prof. Dr.-Ing. A. Luke, Prof. Dr.-Ing. Dr.h.c. D. Mewes, Dipl.-Ing. G. Rohlfing, Dipl.-Ing. M. Reichwage

CO_2 as a function of the pressure difference are shown in Figure 9 for two rotational frequencies. The variable and constant parameters remain the same as given for the volume flow. η_T runs degressively (if $\dot{\alpha} \leq 0.25$) or parabolically (if $\dot{\alpha} > 0.25$) in dependence of the pressure difference. Hence, there is an optimal pressure difference. By increasing $\dot{\alpha}$, η_T is decreased and the optimum is displaced to lower Δp_{MPP}. Decreasing n from 2200 to 1500 min^{-1} makes η_T increase at low and middle Δp_{MPP}, but decrease at high Δp_{MPP}.
The isothermal efficiency is negatively affected by the higher solubility, exept at n=1500 min^{-1} and $\dot{\alpha} \approx 0$, where the conveyed volume flow of oil/CO_2 is higher. At low rotational frequency, η_T of oil/CO_2 is decreased stronger (for $\dot{\alpha} > 0$) compared to n=2200 min^{-1}, since the relative loss volume flows are higher.

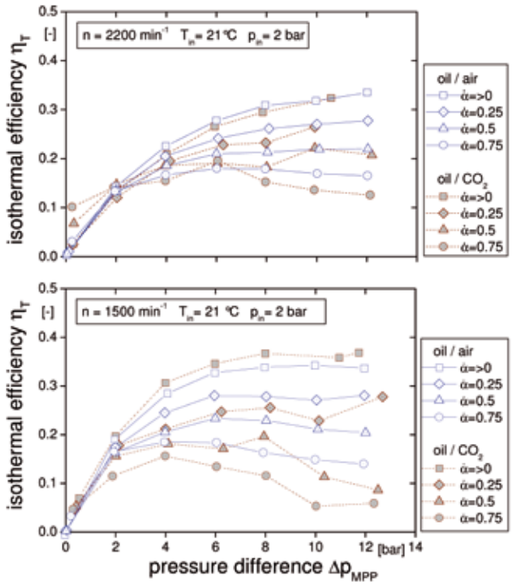

Figure 9: Measured isothermal efficiency for oil/air and oil/CO_2 as a function of the pressure difference at n=2200 and 1500 min^{-1}

In order to examine the volatile volume flow, the two-phase volume flow of oil/air and oil/CO_2 is drawn vs. time in Figure 10. The gas volume flow fraction is varied between 0 and 0.9. The pressure difference and the rotational frequency are constant.

$\dot{V}$ of oil/CO_2 is found to be much lower (for $\dot{\alpha}$=0.25 and $\dot{\alpha}$=0.9) and more volatile (for $\dot{\alpha}$=0.9) in time than oil/air. Thus, high pressure differences and big fractions of highly soluble gases must be regarded as critical operation points of twin-screw MPPs.

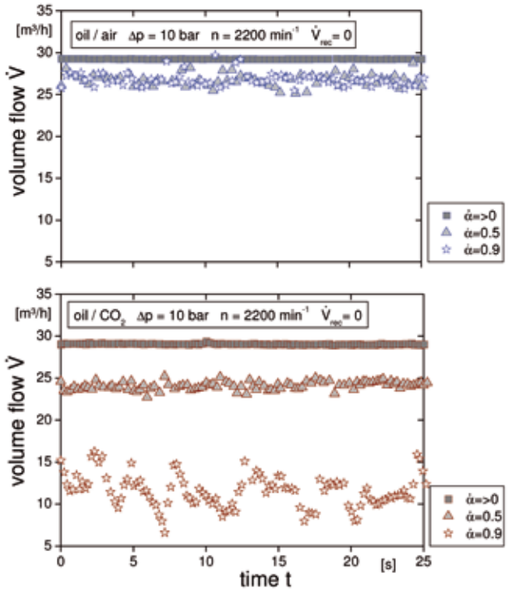

Figure 10: Measured volume flow of oil/air and oil/CO_2 vs. time at 10 bar pressure difference and n=2200 min^{-1}

The influence of internal sorption phenomena on the flow characteristics are regarded now.

4.2 Flow characteristics

The flow characteristics in the inlet and outlet pipe are visualised as longitudinal vertical cut views. The flow patterns and the gas volume fraction over time of 15 s are pictured in Figure 11 by variations of n and $\dot{\alpha}$ at constant Δp.

In the inlet pipe, the flow pattern is stratified at low n and wavy at high n. Decreasing of the (visible) gas volume fraction by increasing n is found for air as well as for CO_2. This induces, that the relative flow velocity of the gas phase is increased, since the gas volume flow fraction is constant. This gives information about the phase fractions in the loss flow. The higher n, the less gas contains the loss volume flow and the faster gas is taken in.

Comparing air to CO_2, the gas volume fraction of CO_2 tends to be lower and the phase interphase is broader. This indicates the passover of less gaseous but more dispersed-in-oil CO_2 (foam).

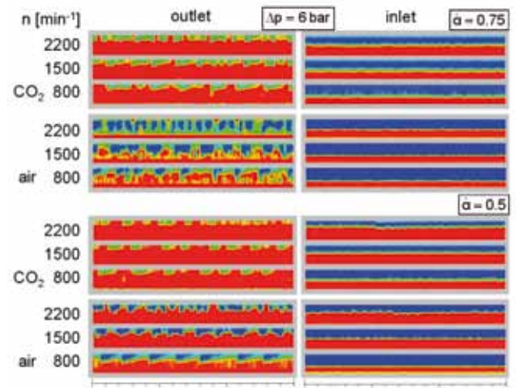

Figure 11: Inlet and outlet two-phase flows of oil/air and oil/CO_2 by variations of n and $\dot{\alpha}$

In the pressure pipe, the gas phase appears as plug and bubble flow. The periodic chamber opening is visible, as the frequency of plugs is increased by rising n. Comparing air to CO_2, the dissolution of gas due to boosting by the MPP is noticeable. The gas volume fraction of CO_2 is much lower than of air. Decreasing $\dot{\alpha}$ is noticeable as decreasing gas volume fraction in the inlet and outlet pipe for both, air and CO_2.

Looking at Figure 12, points out the influence of the pressure difference on the inlet and outlet oil/CO_2 flow characteristics.

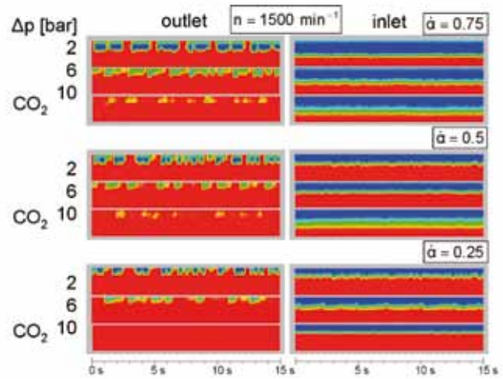

Figure 12: Two-phase flows by variations of Δp and $\dot{\alpha}$

The higher Δp, the more foam appears in the inlet (for $\dot{\alpha} \geq 0.5$), indicating the phase fractions of the loss volume flow. In the outlet, the visible gas fraction is decreased by rising Δp, since the compression is higher and more gas is soluble at higher pressure. At Δp=10 bar, even no gas phase appears in the outlet pipe.

At the same pressure difference, less air than CO_2 is dissolved inside the MPP, which is shown by means of Figure 13. Even at n=2200 min^{-1}, more air appears in the loss volume flow than CO_2 appears at n=1500 min^{-1} which is due to the lower dissolution.

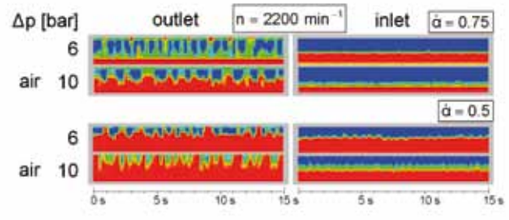

Figure 13: of oil/air and oil/CO_2 vs.

Comparing the experimental results of the flow characteristics to the calculated air and CO_2 volume flow fractions at the outlet, Figure 14, shows good agreement.

By increasing $\dot{\alpha}_{in}$ or decreasing Δp_{MPP}, the calculated $\dot{\alpha}_{out}$ as well as the visible gas volume fraction in the outlet pipe is increased. If dissolution is

Dipl.-Wirtsch.-Ing. T. Groth, Dipl.-Wirtsch.-Ing. F. Hatesuer, Prof. Dr.-Ing. A. Luke, Prof. Dr.-Ing. Dr.h.c. D. Mewes, Dipl.-Ing. G. Rohlfing, Dipl.-Ing. M. Reichwage

considered, $\dot{\alpha}_{out}$ is lower than without dissolution, and for $\dot{\alpha}_{in}$ below the dissolvable inlet gas volume flow fraction (Eq. 21) no gas appears in the outlet pipe. For CO_2, $\dot{\alpha}_{out}$ is much smaller than for air, as the solubility is higher.

Comparing e.g. Δp_{MPP}=6 bar and $\dot{\alpha}_{in}$=0.75 to the experimental results of CO_2, indicates that gas appears even at $\dot{\alpha}_{in}$=0.5 although $\dot{\alpha}_{out}$=0 is calculated. Hence, the equilibrium of vapour and liquid (VLE) is not realized and less gas than soluble is actually dissolved.

Assuming VLE however, the calculated $\dot{\alpha}_{out}$ for CO_2 increases strongly once exceeded the maximum soluble $\dot{\alpha}_{in}$. This affects the flow characteristics in the outlet pipe heavily.

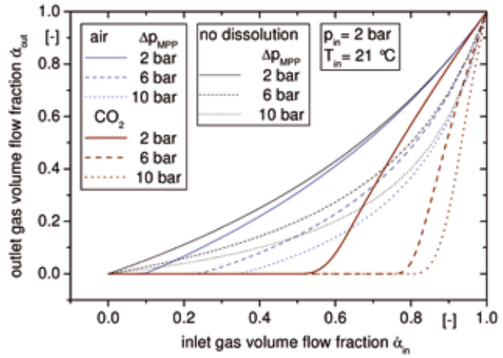

Figure 14: Calculated air and CO_2 volume flow fractions at the outlet in dependence of the inlet and outlet conditions

The influence on the flow pattern and the pressure loss in the pressure side pipework can be estimated by means of the presented dissolution model.

5 CONCLUSIONS

The solubility of gas in oil affects the conveying process of twin-screw pumps, since dissolving and degassing occur in the chamber and gap flows. This exerts an influence on the loss flow and the delivering performance, which is investigated experimentally for two-phase mixtures of oil, air and carbon dioxide. The volume flow as well as the isothermal efficiency are decreased for CO_2 compared to air.

Calculating the solubility by means of the model by Predictive-Soave-Redlich-Kwong indicates the highest solubility for CO_2 and the lowest for air. The solubility of methane is in the middle of both.

Looking at the flow characteristics in the inlet and outlet pipe, visualized by means of an electrical capacitance tomography system, gives information about the behaviour of the gas phase. The gas phase is either conveyed or dissolved or passed over within the loss flow.

In the inlet pipe, the gas volume fraction is decreased by rising the rotational frequency or reducing the pressure difference, which is due to less gas volume passing over within the loss flow.

In the outlet pipe, the gas fraction appears in terms of periodic plugs, whose frequency is increased by rising the rotational frequency. Increasing the pressure difference reduces the gas volume fraction by higher compression and dissolution. Comparing CO_2 to air, the gas fraction of CO_2 is much smaller and may even disappear, as it is dissolved completely.

Comparing the experimental results of the flow characteristics to the calculated dissolution by the MPP, shows good agreement. Only at high inlet gas volume flow fractions, the outlet gas volume flow fraction is underestimated, since equilibrium of saturation is not reached actually.

By means of the dissolution model, the outlet flow pattern and gas fraction are predictable and pipeline operation parameters like the inlet pressure e.g. can be optimized.

ACKNOWLEDGEMENTS

The paper was generated within the scope of the joint project ("Verbundprojekt"): German-Russian cooperation – MPT fundamental Research on Multiphase Technology in Offshore and Onshore Production. Appreciation is expressed to MPT e.V., the industry partners Wintershall AG and Joh. Heinr. Bornemann GmbH and to the university partners for their support. Appreciation is extended in particular to the Federal Ministry for Economics and Technology (BMWi) and the Federal Ministry for Education and Research (BMBF) for funding the project.

REFERENCES

1. Quast, R., Rohlfing G., Seeger D.: Anwendungsgebiete moderner Schraubenspindelpumpen; Pumpen und Kompressoren aus Deutschland, Harnisch Nürnberg, 20-26, 1998

2. Karge V.: Schraubenspindelpumpen zur Förderung von Multiphasengemischen; Pumpen Vakuumpumpen und Kompressoren, 14-20, 1988

3. Salis, J. de, Marolles, C. de, Schachenmann, A., Multiphase pumps for marginal oil fields, WORLD PUMPS, 38-41, July 1994

4. Müller-Link, D., Rohlfing, G., Linck, R., Brown field revitalization using small twin-screw multiphase pumps, Proceedings of the BHR Group, 117-124, 6th North American Conference on Multiphase Technology, Banff, Canada, June 4-6, 2008

5. Vauth, T.: Mehrphasenpumpen im Netzbetrieb; PhD Thesis, University of Hannover, Hannover 2005

6. Aleksieva, G., Scharf, A., Mewes, D., Rohlfing, G., Reichwage, M., Multiphase Transport with Conventional and Newly Designed Twin Screw Pumps in a Pipeline Network, Proceedings of the 5th Joint ASME/JSME Fluids Engineering Conference, 779-786, San Diego, California, USA, July 30-August 2, 2007

7. Räbiger, K., Maksoud, T. M. A., Ward, J., Hausmann, G., Theoretical and experimental analysis of a multiphase screw pump, handling gas-liquid mixtures with very high gas volume fractions, Experimental Thermal and Fluid Science 32, 1694-1701, 2008

8. Aleksieva, G.: Förderverhalten von Mehrphasenpumpen mit variabler Spindelsteigung; PhD Thesis, University of Hannover, Hannover 2008

9. Mewes, D., Aleksieva, G., Scharf, A., Luke, A.: Modelling Twin-Screw Multiphase Pumps – A Realistic Approach to Determine the Entire Performance Behaviour, Proc. 2nd Int. EMBT Conf., Hannover, Germany, April 16-18, 2008

10. Nakashima, C. Y., Junior S. d. O., Caetano E. F.: Thermodynamic model of a twin-screw multiphase pump; ASME ETCE, Houston, 2002

11. Hellmann, D.-H., Gegenüberstellung von Druckerhöhung und Entspannung in Mehrphasenpumpen für viskose Medien, VDI Berichte 1251, 211-241, 1996

12. Baehr, H. D., Thermodynamik, 8. Auflage, Springer-Verlag, 1992

13. Borchers, H. et al., Landolt-Börnstein, 6. Auflage, 4. Band Technik, 4. Teil Wärmetechnik, Bandteil c, Teil 1 Absorption in Flüssigkeiten, Springer Verlag Berlin, Kap. 3, 1976

14. Horstmann, S., Fischer, K., Gmehling, J., Application of PSRK for Process Design, Chem. Eng. Comm. 192, 336-350, 2005

15. Holderbaum, T., Gmehling, J., PSRK: A Group Contribution Equation of State Based on UNIFAC, Fluid Phase Equilibria 70, 251–265, 1991

16. Gmehling, J., Kolbe, B., Thermodynamik, VCH Verlagsgesellschaft Weinheim, 1992

17. VDI Wärmeatlas, 10. bearbeitete, erweiterte Auflage, Springer-Verlag Berlin Heidelberg New York, 2006

18. Rohlfing, G.: Pumpverfahren zum Betreiben einer Multiphasen-Schraubenspindelpumpe und

Pumpe; Patentschrift DE 4316735 C2, Obernkirchen 1996

19. Georgi, W., Metin, E., Einführung in LabVIEW, Fachbuchverlag Leipzig, Carl Hanser Verlag, 2006

20. Xie, C. G., Reinecke, N., Beck, M. S., Mewes, D., Williams, R. A., Electrical tomography techniques for process engineering applications, The Chem. Eng. J. 56, 127-133, 1995

21. Scharf, A., Rausch, T., Aleksieva, G., Reichwaage, M., Mewes, D.: Effect of gap flows inside a multiphase screw pumps on the conveying characteristics; Int. Conf. on Multiphase Flow, ICMF 2007, Leipzig, Germany, July 9-13, 2007

22. Rausch, T.: Thermofluiddynamik zweiphasiger Strömungen in Schraubenspindelpumpen; PhD Thesis, University of Hannover, Hannover 2006

23. Scharf, A., Aleksieva, G., Lewerenz, J., Reichwage, M., Mewes, D.: Pressure build-up and gap flows in multiphase screw pumps, 6th North American Conference on Multiphase Technology, Banff, Canada, June 4-6, 2008

24. Scharf, A.: Untersuchung des Förderprozesses von Gas-Flüssigkeitsgemischen in Schraubenspindelpumpen, PhD Thesis, Leibniz Universität Hannover, 2009

25. Groth, T., Reichwage, M., Mewes, D., Luke, A., Effects of dissolving and degassing phenomena on multiphase oil and gas boosting, Proceedings of the BHR Group, 99-113, 14th Int. Conf. on Multiphase Production Technology, Cannes, France, June 17-19, 2009

26. Hatesuer, F., Groth, T., Reichwage, M., Luke, A., Experimental investigation on dissolving and degassing phenomena in two-phase flows of oil and gas, Proceedings of the 5th European-Japanese Two-Phase Flow Group Meeting, Spoleto, Italy, September 21-25, 2009

27. Groth, T., Hatesuer, F., Reichwage, M., Luke, A., Visualisation of pressure induced degassing in two-phase flows of oil and gas, Proceedings of the 5th European-Japanese Two-Phase Flow Group Meeting, Spoleto, Italy, September 21-25, 2009

28. Fredenslund, A., Jones, R. L., Prausnitz, J. M., Group-Contribution Estimation of Activity Coefficients in Nonideal Liquid Mixtures, AIChE J. 21, 6, 1086-1099, 1975